Journal of The Electrochemical Society, **160** (2) F90-F93 (2013)
0013-4651/2013/160(2)/F90/4/$28.00 © The Electrochemical Society

Performance and Stability of $LaSr_2Fe_2CrO_{9-\delta}$-Based Solid Oxide Fuel Cell Anodes in Hydrogen and Carbon Monoxide

D. M. Bierschenk,[a,*] J. M. Haag,[b] K. R. Poeppelmeier,[b] and S. A. Barnett[a,*,z]

[a]*Department of Materials Science and Engineering, Northwestern University, Evanston, Illinois 60208, USA*
[b]*Department of Chemistry, Northwestern University, Evanston, Illinois 60208, USA*

Composite solid oxide fuel cell (SOFC) anodes consisting of $LaSr_2Fe_2CrO_{3-\delta}$ (LSFeCr) and $Gd_{0.1}Ce_{0.9}O_{2-\delta}$ (GDC) were evaluated during operation on H_2, H_2O-Ar-H_2, CO, and CO-H_2 mixtures. Impedance spectroscopy studies showed three different electrode processes that varied in importance with temperature and fuel composition. The primary impedance response peaked at ∼2 Hz and followed a similar dependence on H_2 partial pressure in both H_2-H_2O-Ar and H_2–CO mixtures. The total anode polarization resistance at 800°C increased by a factor of ∼2 on going from pure H_2 fuel to pure CO.
 [DOI: 10.1149/2.032302jes]

Manuscript submitted July 27, 2012; revised manuscript received November 8, 2012. Published December 4, 2012.

Solid oxide fuel cells (SOFCs) are well suited to replace coal combustion technologies because higher conversion efficiencies can be achieved and the exhaust gas is not diluted with nitrogen, an important consideration for carbon sequestration.[1] There is also considerable interest in using SOFCs with bio-derived syngas fuel, which has a H_2 and CO-rich composition similar to coal syngas. The preferred SOFC anode materials, Ni-cermets, are susceptible to coking in many coal- and bio-derived syngas compositions,[2] and exhibit higher anode polarization resistance $R_{P,A}$ in CO-rich coal gas fuel than in H_2–rich fuels.[3,4] Ni-based anodes are also poisoned by common coal gas impurities such as arsine, phosphine, and hydrogen sulfide.[5,6] These problems can be largely avoided by implementing fuel processing measures, but not without sacrificing the overall power plant cost-effectiveness and efficiency.

A number of conducting-oxide anode materials have been proposed as alternatives to Ni-based anodes.[7–15] The results often show improved tolerance to sulfur poisoning, reduced tendency for carbon deposition in hydrocarbons, and good stability under redox cycling. An example is $LaSr_2Fe_2CrO_{9-\delta}$ (LSFeCr),[16,17] a mixed conductor under typical anode conditions that exhibits little degradation in 22 ppm H_2S, good redox stability, and polarization resistance of ∼ 0.2 Ωcm^2 at 800°C in humidified hydrogen.[18–20] Preliminary results on polarization resistance, stability, and coking behavior in surrogate coal gas fuel compositions have been reported.[21] In order to understand anode behavior in such complex fuel mixtures, experimental data on simpler fuels, particularly H_2/H_2O and H_2/CO, would be useful. Such data is not available for LSFeCr. Indeed, only limited results have been reported on the characteristics of other oxide anodes in H_2 and CO.[21–25]

The present paper describes a study of the LSFeCr anode polarization characteristics in various H_2- and CO-containing mixtures. In particular, a comparison of impedance spectroscopy results versus H_2 partial pressure in H_2/H_2O/Ar and H_2/CO mixtures is used to assess the role of CO in the anode electrochemical oxidation process.

Experimental

Synthesis of Anode Materials and Cells.— The SOFCs were fabricated on $La_{0.9}Sr_{0.1}Ga_{0.8}Mg_{0.2}O_{3-\delta}$ (LSGM) electrolyte supports that had thin $La_{0.4}Ce_{0.6}O_2$ (LDC) barrier layers on the anode side. $La_{0.6}Sr_{0.4}Fe_{0.8}Co_{0.2}O_{3-\delta}$ (LSCF)–$Gd_{0.1}Ce_{0.9}O_2$ (GDC) cathodes were used with LSCF cathode current collectors. The synthesis of the oxide anode material and cell fabrication are detailed below. The cells had a diameter of ∼1.5 cm, an electrolyte thickness of ∼0.3–0.4 mm, and electrode functional-layer thicknesses of 20–30 μm. The anode and cathode areas, both 0.5 cm^2, defined the cell active area.

The LSGM electrolyte powder was prepared via solid-state reaction. Stoichiometric quantities of La_2O_3, $SrCO_3$, Ga_2O_3, and MgO were mixed and calcined at 1250°C for 12 h. The resulting solid was ground, sieved, mixed with poly(vinyl butyral) (PVB) and pressed into 19 mm diameter pellets weighing 0.45 g. The LDC layer was applied by drop-coating a colloidal solution of LDC to one side of bisque-fired (1200°C for 4 h) LSGM pellets. The resulting structures were sintered at 1450°C for 6 h.

The anode material, LSFeCr, was prepared by solid-state reaction. Appropriate quantities of La_2O_3, $SrCO_3$, Cr_2O_3, and Fe_2O_3 were mixed and calcined at 1300°C for 6 h to form LSFeCr. The single-phase perovskite structure was confirmed with powder X-ray diffraction. The composite anode powder was prepared by mixing this powder with commercial GDC (NexTech) at a 1:1 weight ratio for 24 h via ball milling. The resulting powder, with an average particle size of ∼1 μm, was dried, ground, sieved, and mixed with a vehicle (V-737, Heraeus Inc., PA) to form an ink. The thick-film anodes were fabricated by screen printing the anode ink onto the LSGM supports. The anodes were fired at 1200°C for 3 h.

The cathode ink was prepared by mixing LSCF powder (Praxair) and GDC (1:1 weight ratio). The mixture was suspended in the V-737 vehicle with a three-roll mill. In a similar fashion, a current collector ink was prepared with pure LSCF. The cathode inks were applied by screen printing and then firing at 1000°C for 3 h. Au current collector grids were applied to both electrodes by screen printing Au ink (Heraeus Inc., PA).

Cell Testing.— Each cell was mounted on an alumina support tube with Ag ink (DAD-87, Shanghai Research Institute of Synthetic Resins). The silver provided the gas seal and a convenient means for electrically connecting to the anode. Fuel was flowed to the anode through a second, smaller-diameter alumina tube mounted concentrically within the alumina support tube. The cathode was exposed to ambient air. Both alumina tubes were supported by a stainless steel manifold, sealed with viton o-rings, as described elsewhere.[26]

Cell tests were started in humidified H_2. After cell performance stabilized, baseline cell characteristics were recorded in 100 sccm dry H_2 or 50 sccm humidified H_2. H_2-H_2O-Ar mixtures with various compositions were used to vary the H_2 partial pressures; the mixtures were flowed through a humidifier to maintain a constant H_2O content of 3%. Mixtures with varying ratios of dry CO and H_2 were also tested. After the gas composition or operating temperature was changed, cells were allowed a minimum of 30 mins to stabilize prior to characterization.

Electrical measurements were recorded with an electrochemical workstation (IM6, Zahner). The electrochemical impedance spectra (EIS) were recorded over a frequency range of 0.1 to 100 kHz using a 20 mV potential amplitude. Most measurements were done with the cell at open circuit potential, but for H_2-CO mixtures, where the lack of H_2O or CO_2 led to high resistances for potentials greater than open circuit, they were done at 500 mV. The cell impedance data was fit using zView (Scribner) or EQUIVCRT by Boukamp. During operation, the cell potential was recorded with a 2420 Keithley Instruments source meter interfaced with LabVIEW.

*Electrochemical Society Active Member.
zE-mail: s-barnett@northwestern.edu

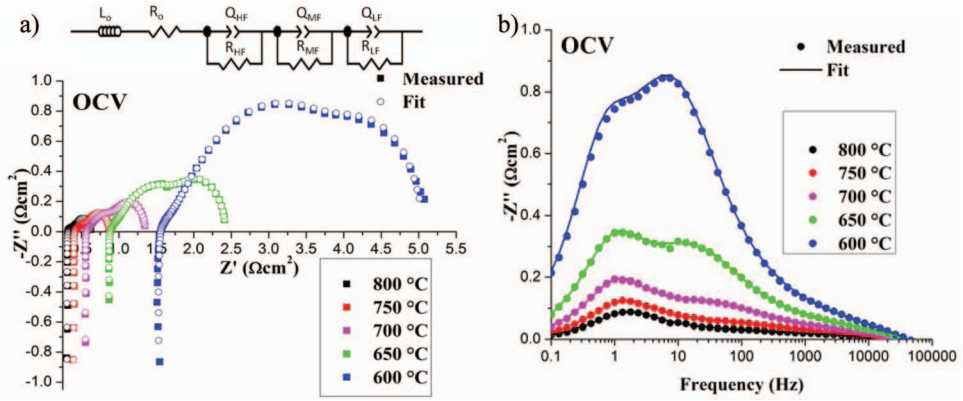

Figure 1. (a) Nyquist and (b) Bode plots of EIS data from an SOFC measured at open circuit at temperatures ranging from 600 to 800°C in humidified H_2. Fits were obtained using an equivalent circuit with three cole elements in series with a resistor and an inductor. The fits yielded root mean square fit values in excess of 0.98.

Results

Effects of Temperature and Hydrogen Partial Pressure.— Figure 1 shows Nyquist and Bode plots of the measured EIS data taken from a typical SOFC at different temperatures. Current-voltage data from similar cells have been reported previously.[20] The Nyquist plot shows that both the first real-axis intercept and the width of the impedance arcs increased with decreasing temperature, reflecting increases in the electrolyte resistance and electrode polarization resistance, respectively. The Bode plot shows three distinct responses: centered at ~1 Hz and termed the low-frequency (LF) response, at ~10 Hz and termed the medium frequency (MF) response, and centered at ~1000 Hz and termed the high frequency (HF) response. The data were fit using an equivalent circuit that included an inductance, a resistance, and three Cole elements that corresponded to the three responses noted above. As shown in Figure 1, the fits were in good agreement with the data.

In order to help separate the cathode portion of the impedance response, an LSCF-GDC cathode symmetric cell on a LSGM support was measured. Figure 2 shows the resulting Bode plot measured at 800°C, compared with that from a full SOFC. The cathode resistance varied from 1.04 Ωcm^2 at 600°C to 0.049 Ωcm^2 at 800°C, with an activation energy of 1.25 eV. The cathode response appeared at ~1000 Hz, the same as the HF element of the full cells; as seen in Figure 2, the cathode was responsible for >50% of the HF response. The MF and LF elements appeared to arise entirely from the anode.

Area-specific resistance values for each process were obtained from the fits to the above data. The ohmic resistance decreased with increasing temperature; these resistances and the corresponding activation energy (0.65 eV) were consistent with conductivity data for LSGM.[27] Figure 3 shows the components of the cell polarization resistance versus inverse temperature, which also followed Arrhenius temperature dependences yielding activation energies $E_{LF} = 0.7$ eV and $E_{MF} = 1.19$ eV. The high frequency feature, attributed mainly to the cathode, is not plotted. The LF anode process is the highest resistance at 800°C, but as the operation temperature decreases, R_{MF} becomes more important due to its higher activation energy. There was no evidence of a response related to gas diffusion.

Figure 4 shows the Nyquist and Bode plots of the EIS data measured at 800°C at open circuit voltage for various H_2 concentrations; the H_2 fuel was diluted with Ar keeping the H_2O concentration at ~3%. Decreasing $p(H_2)$ increased mainly the low frequency response, providing further clear evidence that this process was at the anode. The frequency where Z″ peaked did not vary with $p(H_2)$. The HF response also increased with decreasing $p(H_2)$, but the increase was only slightly greater than the measurement/fitting accuracy. Thus, if there was an anode process, in addition to the cathode process, at this frequency, it was rather small. The EIS data were fit using the

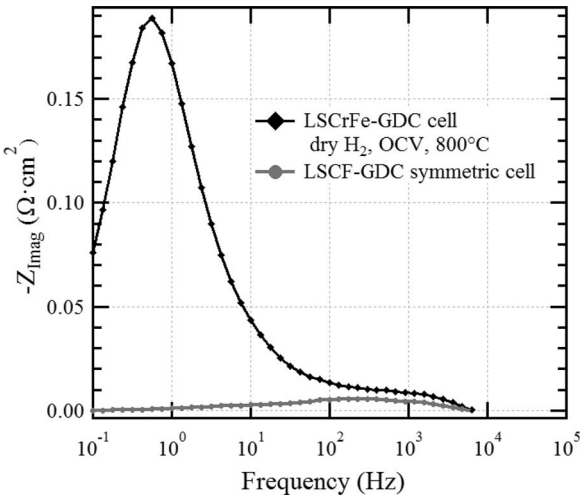

Figure 2. Bode plots from a LSCF-GDC symmetric cell and a full SOFC, both measured at 800°C at open circuit voltage.

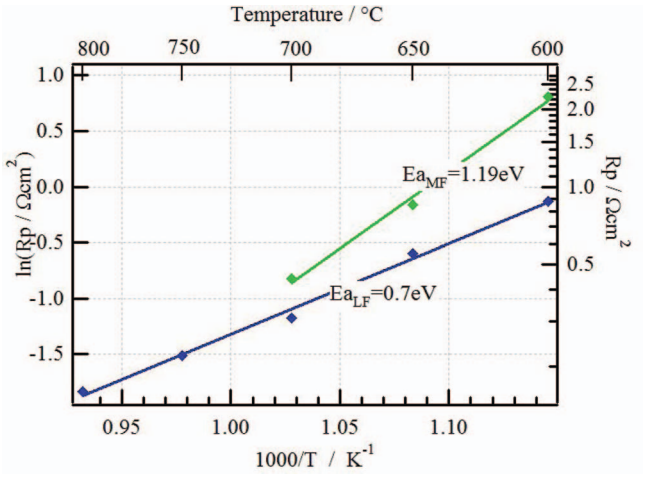

Figure 3. Area specific resistances versus temperature for the medium frequency and low frequency elements, obtained by fitting the equivalent circuit model to the measured impedance data as shown in Figure 1. Note that the high and medium frequency response could not be resolved above 700°C.

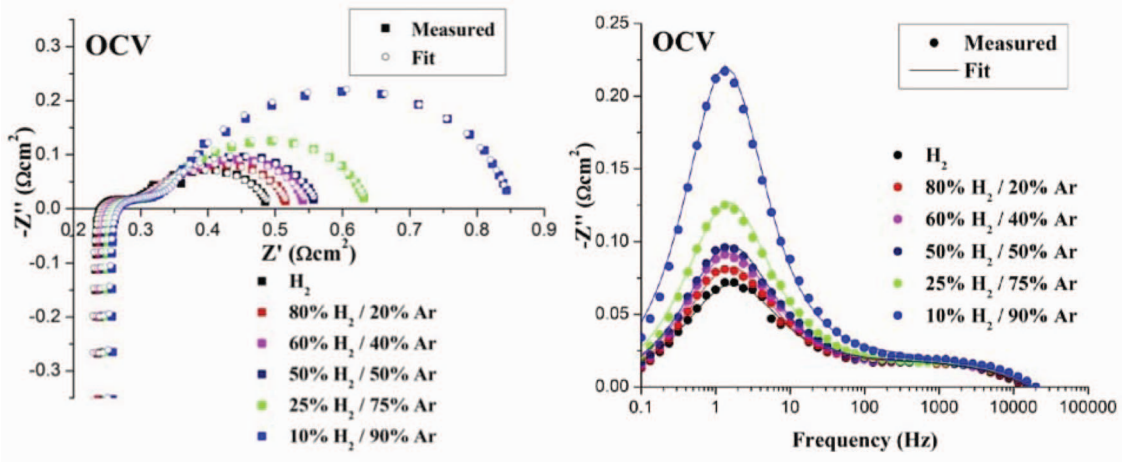

Figure 4. (a) Nyquist and (b) Bode plots measured and fitted for a SOFC at 800 °C at open circuit voltage with different H2 to Ar fuel ratios.

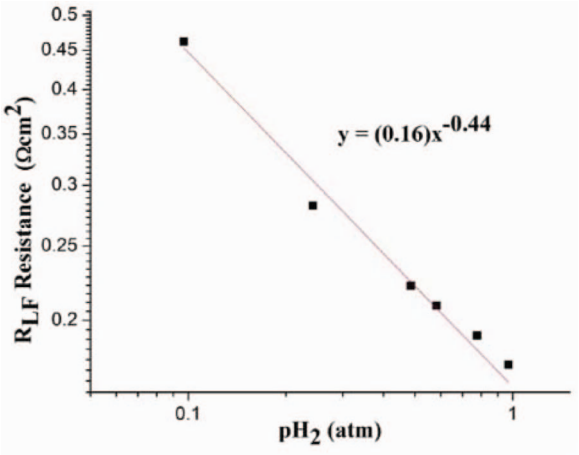

Figure 5. RLF and p(H2) obtained from fits to the EIS data in Figure 4. The line shows the best power law fit obtained, with the expression indicated.

equivalent circuit noted above, but the MF element was omitted as this response was negligibly small at 800°C. The resulting R_{LF} values are shown plotted versus p(H_2) in Figure 5. The best-fit power-law exponent was 0.44, a value that suggests an electrochemical process rather than gas diffusion, which has a power law exponent of 1.[4]

CO/H_2 Fuel Mixtures.— Cell tests were also carried out in H_2-CO fuel mixtures, with no H_2O and CO_2, in order to minimize any shift reactions that could alter the H_2/CO ratio. Current-voltage data reported previously for these conditions showed that cell resistance increased and peak power density decreased with increasing CO content.[21] Figure 6 shows the EIS data recorded for a cell operated on various H_2/CO ratios. The measurements were done at 500 mV, since measurements at open circuit showed inordinately high R_p values due to the lack of product gases (H_2O and CO_2). Temperature dependent data could not be obtained in CO-laden fuels due to an increased threat of coking below 800°C.[21] The EIS data showed a substantial increase in the anode response at ∼2 Hz with decreasing H_2 content.

Figure 7 displays the LF resistance, obtained from fits to the data in Figure 6, versus H_2 content. The LF resistance, the main constituent of $R_{P,A}$, increased by ∼2 times on going from pure H_2 to pure CO. Figure 7 also shows a comparison with the resistance $R_{LF} = 0.16\ (p_{H2})^{-0.44}$ Ωcm^2 obtained from the above H_2-H_2O-Ar dilution experiments (Figures 4 and 5). The absolute values are somewhat different, as expected due to cell-to-cell variations, the presence of 3% H_2O in one case, and the different measurement potential. However, the trend with H_2 partial pressure is quite similar over much of the fuel composition range. This suggests that H_2 plays a dominant role in determining the polarization resistance for H_2-rich fuels. Only at H_2 concentrations < 35% does $R_{P,A}$ for H_2-CO deviate from the H_2 partial pressure power-law dependence, indicating that CO plays an important role.

Discussion

The present results show that the main LSFeCr-anode impedance response is centered at the relatively low frequency of ∼1 Hz, a range often seen for a gas diffusion process, but the strong temperature dependence shows that it was not gas diffusion. One possible explanation for the low frequency is "chemical capacitance" associated with changes in oxygen content of LSFeCr with potential. This term is commonly invoked in the ALS model describing mixed ionically- and electronically-conducting oxide cathodes where the oxygen content varies substantially with effective oxygen pressure,

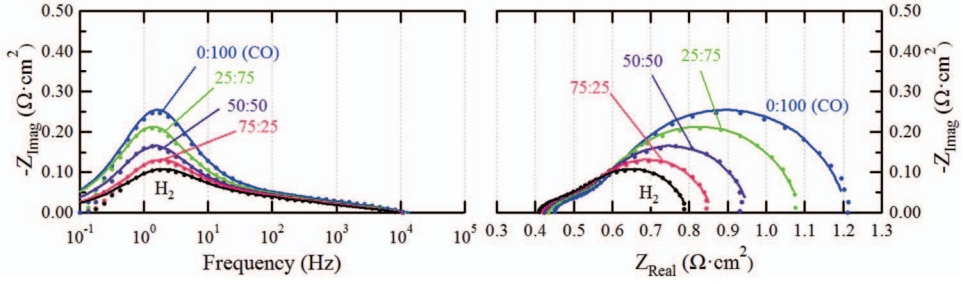

Figure 6. Bode (left) and Nyquist (right) plots of EIS data (symbols) and fit (lines) for a cell operated at 800°C and 500 mV on various H_2/CO ratios.

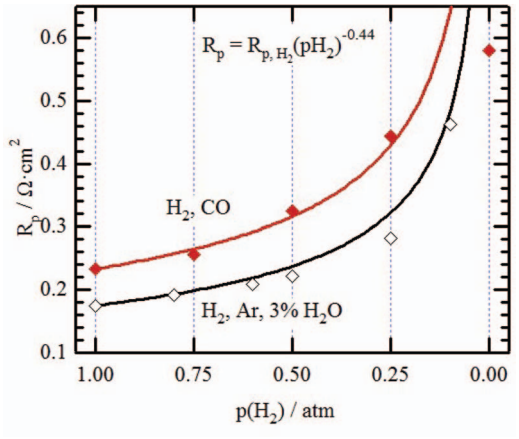

Figure 7. Resistance of the LF response versus H_2 content in H_2-H_2O-Ar (open symbols, from Figure 4) and H_2/CO mixtures (closed symbols). The curves show the dependences expected for a power law with exponent of −0.44.

but may be applicable to LSFeCr anodes because their oxygen content varies strongly with p(O_2).[28,29] A similar low-frequency response was reported for infiltrated (La,Sr)(Cr,Mn)O_3 anodes that also showed substantial oxygen loss under fuel conditions.[30]

For comparison, prior work on (La,Sr)CrO_3 anodes showed a main EIS response at ∼100 Hz, higher than the present LSFeCr anodes.[22] This may be explained by a lower chemical capacitance for (La,Sr)CrO_3, because it exhibits less oxygen loss at low effective oxygen pressure. On the other hand, the response at ∼100 Hz showed a similar H_2 pressure dependence, $(p_{H2})^{0.5}$, but with a substantially larger activation energy of 1.12 eV. (La,Sr)CrO_3 also exhibited a lower-frequency feature, but only at very low p(H_2), suggesting that it was related to gas diffusion.

The oxide anode results can also be compared with literature data for Ni-YSZ anodes operated with H_2 and CO. For the present anodes, switching from H_2 to CO increased $R_{P,A}$ by ∼2 times. This general trend agrees with that observed for Ni-YSZ, where the charge transfer resistance increased by a factor of ∼2 in one case and ∼10 in another on switching from H_2 to CO.[3,31]

Conclusions

EIS data for SOFCs with LSFeCr-GDC anodes were evaluated in varied H_2-H_2O-Ar and CO/H_2 mixtures. In humidified hydrogen, the anode exhibited a polarization resistance of 0.26 Ωcm^2 at 800°C. The dominant impedance response was at ≈1 Hz; its resistance varied with an activation energy of 0.7 eV and as $(p_{H2})^{-0.44}$. $R_{P,A}$ at 800°C increased by a factor of ∼2 on going from pure H_2 to pure CO fuel. The variation of the LF response with p_{H2} was very similar for the H_2-H_2O-Ar and CO/H_2 mixtures for H_2-rich fuels, suggesting that H_2 oxidation was the dominant anode process. For low H_2 and high CO content, the effect of CO oxidation became evident.

Acknowledgments

The authors gratefully acknowledge support from the National Science Foundation (Grant # CBET-0854223) and the Department of Energy (Grant # DE-FG02-05ER46255).

References

1. R. J. Kee, H. Zhu, A. M. Sukeshini, and G. S. Jackson, *Combustion Science and Technology*, **180**, 1207 (2008).
2. B. Novosel, M. Avsec, and J. Macek, *Mater. Tehnol.*, **42**, 51 (2008).
3. Y. Jiang and A. V. Virkar, *J. Electrochem. Soc.*, **150**, A942 (2003).
4. A. Leonide, S. Hansmann, A. Weber, and E. Ivers-Tiffée, *J. Power Sources*, **196**, 7343 (2011).
5. M. J. Zhi, X. Q. Chen, H. Finklea, I. Celik, and N. Q. Q. Wu, *J. Power Sources*, **183**, 485 (2008).
6. Y. Matsuzaki and I. Yasuda, *J. Electrochem. Soc.*, **147**, 1630 (2000).
7. A. Atkinson, S. Barnett, R. J. Gorte, J. T. S. Irvine, A. J. Mcevoy, M. Mogensen, S. C. Singhal, and J. Vohs, *Nature Materials*, **3**, 17 (2004).
8. C. W. Sun and U. Stimming, *J. Power Sources*, **171**, 247 (2007).
9. J. B. Goodenough and Y.-H. Huang, *J. Power Sources*, **173**, 1 (2007).
10. J. M. Haag, B. D. Madsen, S. A. Barnett, and K. R. Poeppelmeier, *Electrochemical and Solid-State Letters*, **11**, B51 (2008).
11. B. D. Madsen, W. Kobsiriphat, Y. Wang, L. D. Marks, and S. A. Barnett, *J. Power Sources*, **166**, 64 (2007).
12. W. Kobsiriphat, B. D. Madsen, Y. Wang, M. Shah, L. D. Marks, and S. A. Barnett, *J. Electrochem. Soc.*, **157**, B279 (2010).
13. D. M. Bierschenk, E. Potter-Nelson, C. Hoel, Y. Liao, L. Marks, K. R. Poeppelmeier, and S. A. Barnett, *J. Power Sources*, **196**, 3089 (2011).
14. Y. Wang, B. D. Madsen, W. Kobsiriphat, S. A. Barnett, and L. D. Marks, *Microsc. microanal.*, **13**, 100 (2007).
15. W. Kobsiriphat, B. D. Madsen, Y. Wang, L. D. Marks, and S. A. Barnett, *Solid State Ionics*, **180**, 257 (2009).
16. M. F. Lu, E. V. Tsipis, J. C. Waerenborgh, A. A. Yaremchenko, V. A. Kolotygin, S. Bredikhin, and V. V. Kharton, *J. Power Sources*, **206**, 59 (2012).
17. S. W. Tao and J. T. S. Irvine, *Chem. Mat.*, **16**, 4116 (2004).
18. V. L. Kozhevnikov, I. A. Leonidov, J. A. Bahteeva, M. V. Patrakeev, E. B. Mitberg, and K. R. Poeppelmeier, *Chem. Mat.*, **16**, 5014 (2004).
19. J. M. Haag, B. D. Madsen, S. A. Barnett, and K. R. Poeppelmeier, *Electrochemical and Solid-State Letters*, **11**, B51 (2008).
20. J. M. Haag, D. M. Bierschenk, S. Barnett, and K. R. Poeppelmeier, *Solid State Ionics*, submitted (2011).
21. D. M. Bierschenk, J. M. Haag, K. R. Poeppelmeier, and S. A. Barnett, *ECS Transactions*, **25**, 2107 (2009).
22. P. Vernoux, *Ionics*, **3**, 270 (1997).
23. M. Gong, D. Bierschenk, J. Haag, K. R. Poeppelmeier, S. A. Barnett, C. Xu, J. W. Zondlo, and X. Liu, *J. Power Sources*, **195**, 4013.
24. M. Cooper, K. Channa, R. De Silva, and D. J. Bayless, *J. Electrochem. Soc.*, **157**, B1713 (2010).
25. D. M. Bierschenk and S. A. Barnett, *J. Power Sources*, **201**, 95 (2012).
26. M. R. Pillai, D. M. Bierschenk, and S. A. Barnett, *Catalysis Letters*, **121**, 19 (2008).
27. J. W. Fergus, *J. Power Sources*, **162**, 30 (2006).
28. S. B. Adler, J. A. Lane, and B. C. H. Steele, *J. Electrochem. Soc.*, **143**, 3554 (1996).
29. J. M. Haag, S. A. Barnett, J. W. Richardson, and K. R. Poeppelmeier, *Chem. Mat.*, **22**, 3283 (2010).
30. G. Kim, S. Lee, J. Y. Shin, G. Corre, J. T. S. Irvine, J. M. Vohs, and R. J. Gorte, *Electrochem. Solid-State Lett.*, **12**, B48 (2009).
31. A. Leonide, SOFC Modelling and Parameter Identification by means of Impedance Spectroscopy, in *Institut für Werkstoffe der Elektrotechnik*, Karlsruhe Institute of Technology, Karlsruhe, Germany (2010).